Morphological Structure of Crystalline Polymer Blend Involving Hydrogen Bonding: Polycaprolactone/Poly(4-vinylphenol) System

Hsin-Lung Chen,*,† Shi-Fang Wang,† and Tsang-Lang Lin‡

Department of Chemical Engineering and Department of Engineering and System Science, National Tsing Hua University, Hsin-Chu, Taiwan 30043, R. O. C.

Received July 13, 1998

ABSTRACT: The importance of crystal growth rate in the morphological formation of strongly interacting crystalline/amorphous polymer blends has been assessed by considering polycaprolactone (PCL)/poly(4-vinylphenol) (PVPh) systems. The effects of composition and molecular weight (MW) on the morphological structure were investigated by small-angle X-ray scattering (SAXS). Blending with PVPh increased the long period associated with the alternating crystalline−amorphous layers. The long period increase was characterized by the thickening of PCL crystals upon blending instead of the swelling of amorphous layers. The extent of extralamellar segregation of PVPh was revealed from the volume fraction of lamellar stacks. Despite the relatively high T_g of PVPh, significant extralamellar segregation of PVPh was observed. The extent of extralamellar segregation increased with PVPh composition for a given molecular weight combination of PCL and PVPh. For a given composition, the blends with PCL molecular weight (M_{PCL}) of 15 800 exhibited a higher extent of extralamellar segregation than the systems with $M_{PCL} = 2600$ and 3800. The extent of segregation was relatively unaffected by the MW of PVPh (M_{PVPh}) for the two molecular weight fractions investigated ($M_{PVPh} = 4000$ and 30 000). Good correlations were found between the extent of extralamellar segregation and crystal growth rate, where slower growth rate led to higher extent of extralamellar segregation. The crystal growth rate of PCL in the blends thus played the dominant role in the morphological formation of PCL/PVPh system.

Introduction

Binary polymer blends can be categorized into amorphous/amorphous, crystalline/ amorphous, and crystalline/crystalline systems based on the crystallizability of the constituents. For the latter two systems where at least one constituent is crystallizable, occurrence of liquid−solid phase separation offers an effective route to produce a wide variety of morphological patterns.[1] In a melt-miscible crystalline/amorphous blend, for example, crystallization is accompanied by the segregation of the amorphous diluent. The morphological pattern is characterized by the distance over which the diluent is segregated, where three basic types of morphology may be generated: (1) interlamellar segregation, where diluent is expelled by a short distance such that it is trapped inside the interlamellar regions, (2) interfibrillar segregation, where diluent is segregated by a larger distance to the regions between the lamellar bundles in spherulites, and (3) interspherulitic segregation, where diluent is rejected out of the spherulites.[1] These morphological patterns represent the diluent dispersion from nanometers for interlamellar segregation to micrometers for interspherulitic segregation. Different scales of dispersion may lead to different properties.

Although the morphological structures of crystalline/amorphous polymer blends have been widely investigated (e.g., refs 1−20), the principles dictating the location of the diluent are still not well understood. It has been suggested that the diluent molecules confined in the interlamellar regions are deformed by the crystals and have lower conformational entropy.[4] An entropic driving force is thus developed, tending to pull diluent molecules out of the interlamellar zones. This entropic force competes against the favorable interaction between the diluent and the amorphous portion of the crystalline polymer in the interlamellar regions. Consequently, exclusion of diluent out of the interlamellar regions may be governed by the magnitude of interaction and the interlamellar distance (which determines the extent that diluent molecules are deformed); both may depend on composition, temperature, and molecular weight (MW). In addition to the thermodynamic consideration, kinetically, the diluent mobility may also be a decisive factor. The competitive effect of diluent diffusivity and crystal growth rate has been suggested to govern the segregation distance.[21] A larger diluent diffusivity and slower crystal growth will lead to a longer segregation distance, and vice versa. The influence of diluent mobility on the morphology has been examined in several studies.[6,16,22] A summary of the results has recently been given by Debier et al.[22] Interlamellar segregation was often observed when T_g of the diluent is similar to or higher than the crystallization temperature (T_c). When T_c becomes higher than T_g of the diluent, interfibrillar or interspherulitic segregation was often observed. However, this simple rule is violated by some systems, implying that a much more complex mechanism controls the morphological formation in the blends.

The roles of both diluent mobility and interaction strength in diluent segregation were recently examined by Talibuddin et al.[16] In the study, poly(ethylene oxide) (PEO) was blended with four amorphous polymers: poly(methyl methacrylate) (PMMA), poly(vinyl acetate)

* To whom correspondence should be addressed.
† Department of Chemical Engineering.
‡ Department of Engineering and System Science.

10.1021/ma9811019 CCC: $15.00
Published on Web 11/26/1998

(PVAc), ethylene−methacrylic acid copolymer (EMAA55), and styrene−*p*-hyroxystyrene copolymer (SHS50). PEO/PMMA and PEO/PVAc represent the weakly interacting systems, where the former has a higher diluent T_g. PEO/EMAA55 and PEO/SHS50 represent the strongly interacting systems, where the former has a lower diluent T_g. The small-angle X-ray scattering (SAXS) analysis indicated that, for the weakly interacting systems, the high-T_g diluent (PMMA) resided exclusively in interlamellar regions whereas the low-T_g diluent (PVAc) was excluded partially into the interfibrillar regions. Therefore, segregation morphology of weakly interacting systems is largely controlled by the diluent mobility. For the strongly interacting blends, the diluents were segregated over a greater distance regardless of their T_g's. It was suggested that the strong interaction significantly reduced the crystal growth rate and consequently promoted the diluent segregation. The length scale of diluent segregation was hence dominated by the crystal growth rate for these systems.

As the development of the universal principle is crucial for effective morphological control of crystalline/amorphous blends, the importance of crystal growth rate in the morphological formation of strongly interacting blends is further assessed in this paper. In the present study, the morphological structure of another strongly interacting system, polycaprolactone (PCL)/poly(4-vinylphenol) (PVPh) blend, is probed by SAXS. PCL and PVPh form a melt-miscible blend through hydrogen-bonding interaction, and PCL is able to crystallize in the blend.[23−25] In the study, the effects of composition, molecular weight of PCL (M_{PCL}), and molecular weight of PVPh (M_{PVPh}) on the morphological structure are examined. The role of crystal growth rate in the morphological formation will be considered in detail in this paper.

Experimental Section

Materials and Sample Preparation. PCL with M_n of 2600 (PCL2K), 3800 (PCL3K), and 15800 (PCL15K) were prepared in the previous study.[26] Two PVPh samples with molecular weight of 4000 (PVPh4K) and 30 000 (PVPh30K) were purchased from Polysciences Inc. Blendings of PCL and PVPh were carried out by solution casting. The blending components were dissolved in tetrahydrofuran (THF) at room temperature yielding a 1 wt % solution. The solution was subsequently poured onto a Petrie dish, and the blend film was obtained after evaporating most THF solvent on a hot plate at ca. 60 °C. The blend film was further dried in vacuo at 60 °C for 24 h.

Samples for SAXS study were prepared by compression molding. The blend obtained from solution casting was compression molded by a hot press at 130 °C for 5 min to yield a disk of ca. 1 mm thick. The sample was then quickly transferred into an oven equilibrated at 30 ± 2 °C for crystallization. Since the SAXS analysis presented in this study requires the spherulites within the sample to be volume filling, crystallization at 30 °C was conducted for 96 h. Optical microscopy confirmed that volume-filling spherulites were obtained through such a crystallization condition.

Bulk Crystallinity Measurements. Bulk crystallinities of semicrystalline PCL/PVPh blends were calculated from the density. The densities were measured by a density gradient column at 23 °C. A calcium nitrate aqueous solution was used to establish the density gradient ranging from 1.07 to 1.28 g/cm^3. The samples used for density measurement were cut directly from the sample disks for SAXS measurement. Crystallinities were calculated by taking the density of PVPh = 1.1667 g/cm^3, the density of totally amorphous PCL = 1.095 g/cm^3, and the density of 100% crystalline PCL = 1.194 g/cm^3.[2]

Melting Point and Crystal Growth Rate Measurements. The melting points of PCL/PVPh blends crystallized at various temperatures were measured by a TA Instrument 2000 differential scanning calorimeter (DSC). The sample was annealed at 130 °C for 3 min followed by quickly cooling at ca. 120 °C/min to the desired crystallization temperature. Crystallization was allowed to proceed for 10 h prior to the melting point measurement. The DSC scanning rate was 20 °C/min.

The spherulite growth was monitored with a Pac Hund polarized optical microscope. The sample was first melted on a Linkam HFS91 hot stage at 130 °C for 3 min. The sample was then quickly transferred to another hot stage equilibrated at 30 °C, and the spherulite growth was monitored. Micrographs were taken at intervals for measuring the spherulite radii (R) at various time periods. The growth rate was calculated from the change of spherulite radius with time, dR/dt.

SAXS Measurement. All SAXS measurements were performed at room temperature (ca. 27 °C). The power of X-ray source was operated at 200 mA and 40 kV. The X-ray source is a 18 kW rotating anode X-ray generator (Rigaku) equipped with a rotating anode Cu target. The incident X-ray beam was monochromated by a pyrolytic graphite, and a set of three pinhole inherent collimators were used so that the smearing effects inherent in slit-collimated small-angle X-ray cameras can be avoided. The sizes of the first and second pinholes are 1.5 and 1.0 mm, respectively, and the size of the guard pinhole before the sample is 2.0 mm. The scattered intensity was detected by a two-dimensional position sensitive detector (ORDELA model 2201X, Oak Ridge Detector Laboratory Inc.) with 256 × 256 channels (active area 20 × 20 cm^2 with ∼1 mm resolution). The sample to detector distance is 4000 mm long. The beam stop is around lead disk of 18 mm in diameter. All data were corrected by the background (dark current and empty beam scattering) and the sensitivity of each pixel of the area detector. The area scattering pattern has been radially averaged to increase the efficiency of data collection compared with one-dimensional linear detector. Data were acquired and processed on an IBM-compatible personal computer. The intensity profile was output as the plot of the scattering intensity (I) vs the scattering factor, $q = 4\pi/\lambda \sin(\theta/2)$ (θ = scattering angle).

Results and Discussion

Figure 1 displays the profiles of Lorentz-corrected intensity (Iq^2) of semicrystalline PCL/PVPh blends with three combinations of M_{PCL} and M_{PVPh}. For all MW combinations, the peak position (q_{max}) shifts toward lower angle with increasing PVPh composition, showing that the long period (L) calculated from the Bragg's law increases. In the lamellar stack model with sharp phase boundary, the long period represents the sum of the crystal thickness (l_c) and the amorphous layer thickness (l_a). Rise in long period may thus stem from the thickening of PCL crystals or the swelling of amorphous layers upon blending with PVPh. Two approaches may be utilized to determine the average thicknesses of the two layers, namely, the one-dimensional correlation function and the interphase distribution function. The one-dimensional correlation function is defined as[27]

$$\gamma(z) = \frac{1}{\gamma(0)} \int_0^\infty I(q) q^2 \cos(qz)\, \mathrm{d}q \qquad (1)$$

where z is the direction along which the electron density is measured. $\gamma(0)$ is just the scattering invariant:

$$Q = \int_0^\infty I(q) q^2\, \mathrm{d}q \qquad (2)$$

Since the experimentally accessible q range is finite,

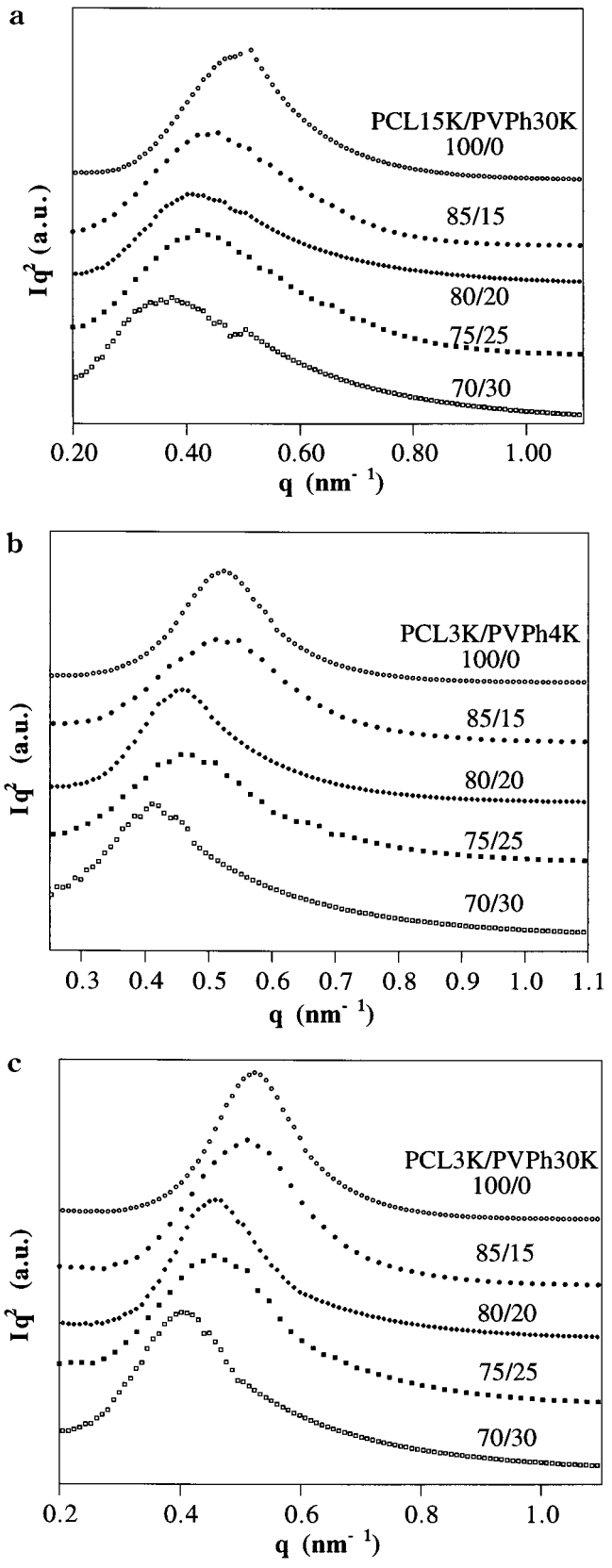

Figure 1. Profiles of Lorentz-corrected SAXS intensity of semicrystalline (a) PCL15K/PVPh30K, (b) PCL3K/PVPh4K, and (c) PCL3K/30K blends. Blend compositions are indicated in the figure.

extrapolation of intensity to both low and high q is necessary for the integrations. Extrapolation to zero q was accomplished by the Debye−Bueche model[28,29]

$$I(q) = \frac{A}{(1 + a_c^2 q^2)^2} \tag{3}$$

where A is a constant and a_c is the correlation length. A and a_c can be determined from the plot of $I(q)^{-1/2}$ vs q^2 using the intensity data at low q region. Extension to large q can be performed using the Porod−Ruland model[30]

$$I(q) = K_p \frac{\exp(-\sigma^2 q^2)}{q^4} + I_{fl} \tag{4}$$

where K_p is the Porod constant, σ is a parameter related to the thickness of crystal/amorphous interphase, and I_{fl} is the background intensity arising from thermal density fluctuation. The values of K_p, σ, and I_{fl} were obtained by curve fitting the intensity profile at high q region.

Determinations of l_c, l_a, and L may be realized by locating the first minimum and maximum in the one-dimensional correlation function.[27] However, a recent study by Santa Cruz et al. showed that the positions of minimum and maximum in the correlation function may be perturbed by the broad size distribution of lamellae.[31] An alternative approach, through the use of the interphase distribution function, was suggested to yield more reliable values of l_c, l_a, and L.[31,32] The interphase distribution function, $g_1(z)$, is defined by the second derivative of $\gamma(z)$:[31−33]

$$g_1(z) = \gamma''(z) \tag{5}$$

Figure 2 presents the interphase distribution functions of PCL15K/PVPh30K blends. The first minimum of $g_1(z)$ provides the value of long period, and the first maximum yields the thickness of either crystalline or amorphous layer. Based on the Babinet's reciprocity theorem,[34] it is not possible to distinguish whether the first maximum corresponds to l_c or l_a. Therefore, the smaller length deduced from the first maximum is denoted by l_1, and the larger length given by $L - l_1$ is denoted by l_2. Figure 3 displays the composition variations of l_1 and l_2 for PCL15K/PVPh30K blend. Both L and l_2 increase while l_1 drops slightly with increasing PVPh composition. Similar composition dependence is identified for other MW combinations.

The assignment of l_1 and l_2 is governed by the magnitude of the linear crystallinity, ϕ_c^{lin}, which is defined as

$$\phi_c^{lin} = \frac{l_c}{L} = \frac{l_c}{l_c + l_a} \tag{6}$$

When the linear crystallinity is lower than 0.5, the crystals contribute to the smaller thickness; thus $l_1 = l_c$ and $l_2 = l_a$. The inverse is true for $\phi_c^{lin} > 0.5$. Provided that the spherulites in the sample are volume-filling, the linear crystallinity is related to the bulk crystallinity, ϕ_c, by

$$\phi_c = \phi_s \phi_c^{lin} \tag{7}$$

where ϕ_s is the volume fraction of lamellar stacks in the sample. Since $\phi_s \leq 1$, eq 7 prescribes that the bulk crystallinity cannot be higher than the linear crystallinity. As a result, the assignment of l_1 and l_2 would be rather straightforward if the bulk crystallinity is greater

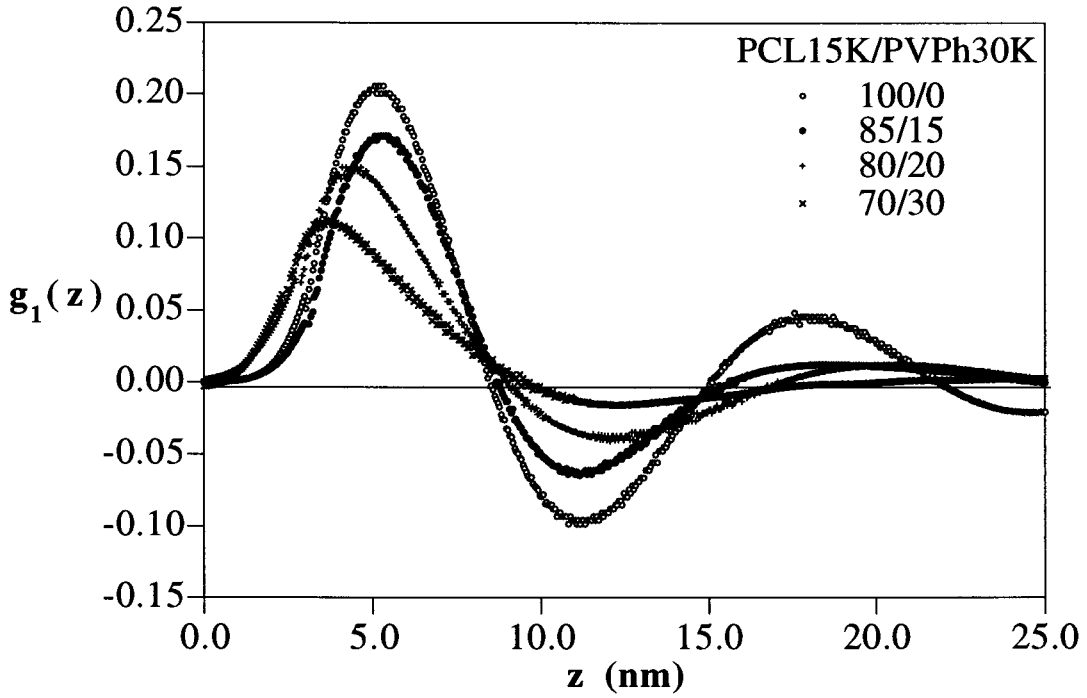

Figure 2. Interphase distribution function of PCL15K/PVPh30K blends. The first maximum yields the thickness of the thinner layer (l_1). The long period (L) is given by the first minimum.

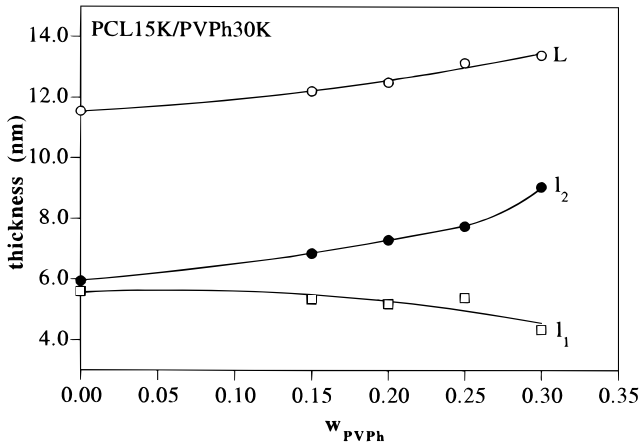

Figure 3. Composition variations of long period and the thicknesses of the thinner layer (l_1) and the thicker layer (l_2) for PCL15K/PVPh30K blends.

than 0.5, because in this case the larger length, l_2, must correspond to the crystal thickness and l_1 to the amorphous layer thickness. The bulk crystallinities of PCL/PVPh were found to lie above 0.5 for the majority of blend compositions investigated ($0.8 \leq w_{PCL} \leq 1.0$). Consequently, we assigned l_1 as the amorphous layer thickness and l_2 the crystal thickness. With such an assignment, the crystal thickness was found to increase with PVPh composition, as can be seen in Figure 3. The effect of blending on crystal thickness has been demonstrated for many systems. In most cases, the crystal thickness was relatively unperturbed by blending.[4,11,35−37] Reduction of crystal thickness has been identified for systems such as PCL/poly(vinyl chloride) (PVC)[20] and PCL/poly(styrene-*co*-acrylonitrile) (SAN).[35] Increase in crystal thickness upon blending has been observed in systems such as PEO/EMAA55 and PEO/SHSS50.[16] The formation of thicker crystals in the blends is attributed to the depression of equilibrium melting point, which is particularly effective in systems involving strong interactions. According to the secondary nucleation theory, the initial crystal thickness is given by[38,39]

$$l_g^* = \frac{2\sigma_e T_m^0}{\Delta h_f^0 (T_m^0 - T_c)} + \delta l \tag{8}$$

where T_m^0 is the equilibrium melting point, σ_e is the fold surface free energy, and Δh_f^0 is the bulk enthalpy of melting per unit volume. δl is given by[39]

$$\delta l = \frac{k_B T_c}{2 b_0 \sigma}\left[\frac{\Delta g_f^0 + 4\sigma/a_0}{\Delta g_f^0 + 2\sigma/a_0}\right] \tag{9}$$

where a_0 and b_0 are the width and thickness of a stem, Δg_f^0 is the bulk free energy of melting per unit volume, and σ is the side surface free energy. At low to moderate degree of supercooling, δl is small compared with $2\sigma_e/\Delta g_f^0$; thus eq 8 reduces to

$$l_g^* \cong \frac{2\sigma_e T_m^0}{\Delta h_f^0 (T_m^0 - T_c)} \tag{10}$$

Equation 10 prescribes that the initial crystal thickness is inversely proportional to the degree of supercooling. Because depression of equilibrium melting point upon blending lowers the degree of supercooling for a given T_c, a larger l_g^* is induced in the blend. The final crystal thickness, according to the notation of Hoffman and Weeks,[38,39] is γ times the initial thickness, viz.

$$l_c = \gamma l_g^* \tag{11}$$

where γ is the so-called "lamellar thickening factor", which can be obtained from the Hoffman−Weeks equation:

$$T_m = T_m^0\left(1 - \frac{1}{\gamma}\right) + \frac{T_c}{\gamma} \tag{12}$$

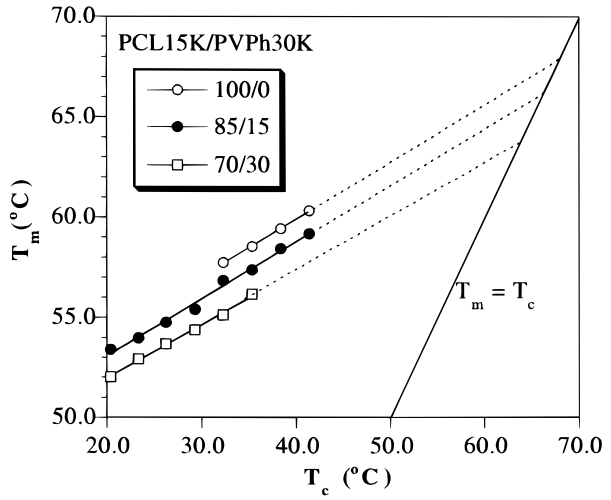

Figure 4. Hoffman−Weeks plot for obtaining the lamellar thickening factor (γ) and the equilibrium melting point (T_m^0) of PCL15K/PVPh30K blends.

Table 1. Lamellar Thickening Factor (γ) and Equilibrium Melting Point (T_m^0) Obtained from the Hoffman−Weeks Plot of PCL15K/PVPh30K Blend

PCL/PVPh	γ	T_m^0(°C)	$\gamma T_m^0/(T_m^0 - T_c)^a$
100/0	3.53	67.8	31.8
85/15	3.50	66.3	32.7
80/20	3.53	64.4	34.6
70/30	3.73	63.7	37.3

[a] T_c = 30 °C.

where T_m is the nonequilibrium melting point corresponding to the crystal thickness of l_c.

To confirm that blending with PVPh did induce the formation of thicker PCL crystals, T_m^0 and γ were determined from the Hoffman−Weeks T_m vs T_c plot for various PCL/PVPh compositions. The slope of the plot yields the value of $1/\gamma$, and the intercept with $T_m = T_c$ line gives the value of T_m^0. The potential problems associated with the use of Hoffman−Weeks plot to extrapolate T_m^0 have been discussed by Hoffman and Miller.[39] At large degree of supercooling, the δl term in eq 8 becomes important, and curvature may be induced in the plot. Figure 4 shows the Hoffman−Weeks plot of PCL15K/PVPh30K blends. Excellent linearities extended over the T_c range investigated are found for pure PCL and the blends. Table 1 lists the values of γ along with the extrapolated equilibrium melting points. The extrapolated T_m^0 of pure PCL is 67.8 ± 1 °C, which closely agrees with the value of 69 ± 1 °C determined by a method independent of the Hoffman−Weeks extrapolation.[40] It can be seen from Table 1 that γ of the blends is about the same as that of pure PCL. The product of γ and $T_m^0/(T_m^0 - T_c)$, which is proportional to the crystal thickness, is also listed. The product increases with increasing PVPh composition, supporting that the blends did contain the thicker crystals.

Once the crystal thickness has been determined, the linear crystallinity, ϕ_c^{lin}, can be calculated by eq 6, and the volume fraction of lamellar stacks can subsequently be obtained by eq 7 with the knowledge of bulk crystallinity. The magnitude of ϕ_s is closely connected with the morphological structure. In the case of complete interlamellar segregation, the whole sample is homogeneously filled with lamellar stacks, so $\phi_s = 1$. A larger extent of extralamellar segregation will result in smaller ϕ_s. Figure 5 plots ϕ_s against the composition. For a given

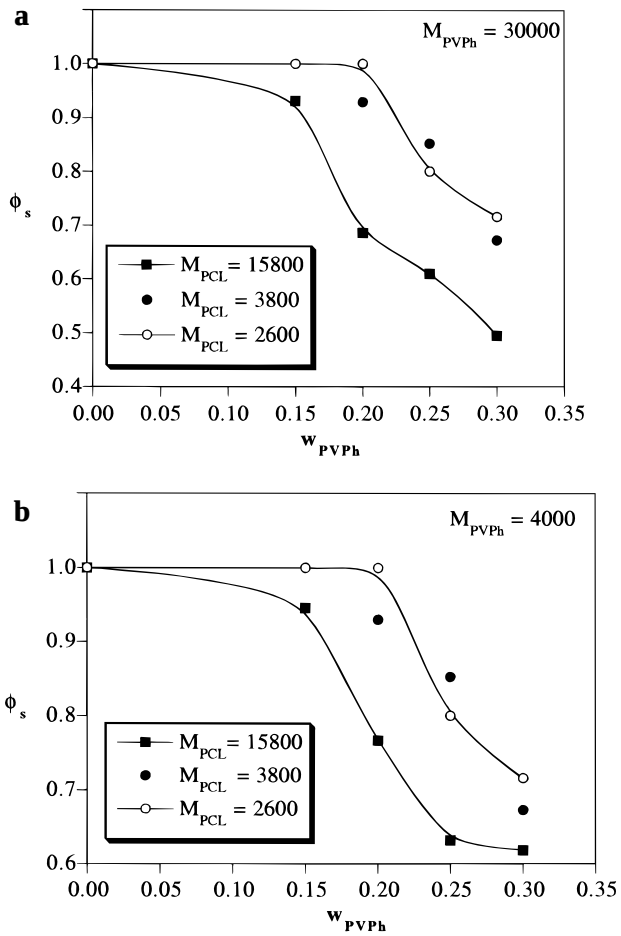

Figure 5. Composition variation of the volume fraction of lamellar stacks (ϕ_s) for (a)PCL/PVPh30K and (b) PCL/PVPh4K blends. Molecular weight of PCL is indicated in the figure.

MW combination, ϕ_s starts to drop notably as the composition of PVPh exceeds 15 or 20 wt %, which means the extent of extralamellar segregation rises with PVPh composition. Because volume-filling spherulites were observed by optical microscopy for all compositions and MW combinations investigated, the extralamellar segregation should be characterized by the morphology of interfibrillar segregation.

The segregation morphology of another PCL system, PCL/PVC, has been reported to be predominantly interlamellar segregation.[1] In a recent study, we observed some extent of interfibrillar morphology for this system.[20] Comparing with PCL/PVC, PCL/PVPh blends actually exhibited a larger extent of extralamellar segregation. This observation cannot be justified from the diluent mobility because the T_g of PVPh is 60 °C higher than that of PVC; the relatively high T_g of PVPh could restrict its segregation distance compared with the segregation of PVC in PCL/PVC systems. Since this was not observed, it means that the morphological formation in PCL/PVPh blends was not governed by the T_g of PVPh.

The effect of M_{PCL} on the morphological structure can also be deduced from Figure 5. For a given composition, the extents of extralamellar segregation are about the same for the blends with M_{PCL} of 2600 and 3800; on the other hand, the blends with M_{PCL} of 15 800 exhibit a larger extent of extralamellar segregation. This observation suggests that the rejection of PVPh is promoted by rising the molecular weight of PCL. The effect of

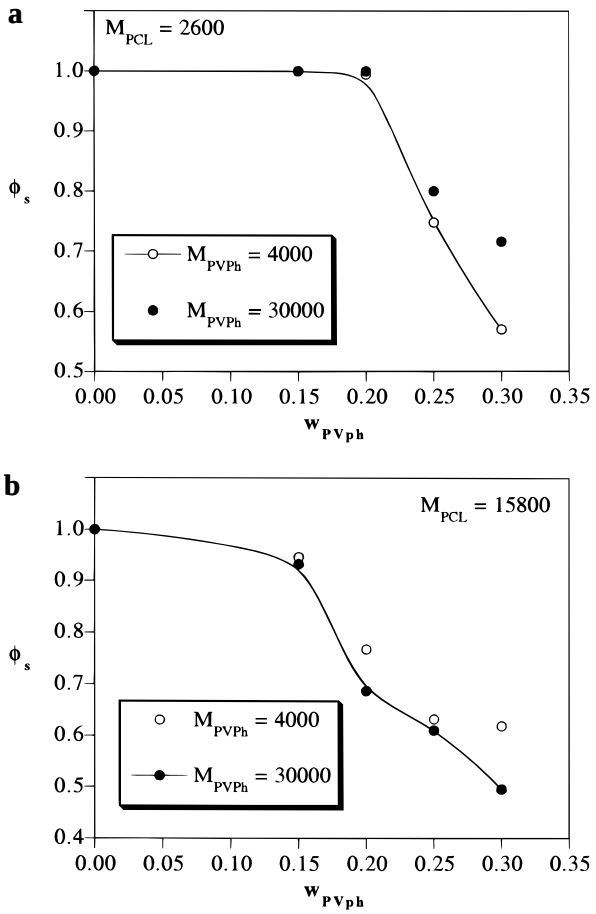

Figure 6. Composition variation of the volume fraction of lamellar stacks (ϕ_s) for (a)PCL2K/PVPh and (b) PCL15K/PVPh blends. Molecular weight of PVPh is indicated in the figure. The error associated with ϕ_s is ±0.02.

M_{PVPh} on the morphological structure is displayed in Figure 6. For a given composition, the extent of extralamellar segregation is approximately the same for the two M_{PVPh} fractions (M_{PVPh} = 4000 and 30 000) investigated.

Summarizing the morphological structure deduced from Figures 5 and 6, the extent of extralamellar segregation of PVPh was found to increase with PVPh composition, the blends with M_{PCL} = 15 800 exhibited a larger extent of extralamellar segregation than the blends with M_{PCL} = 2600 and 3800, and the molecular weight of PVPh has little influence on the morphological structure for the two M_{PVPh} fractions investigated. It has been suggested that, for the systems involving strong interaction such as hydrogen bonding, the formation of morphological structure is predominantly governed by the crystal growth rate.[16] The large negative χ in strongly interacting systems induces a large depression in crystallization driving force and thus reduces the crystal growth rate considerably. Because of the slow growth rate, the amorphous diluent can diffuse out more easily and avoids being trapped inside the interlamellar regions. Thus, a stronger depression in growth rate may result in a larger extent of extralamellar segregation in strongly interacting systems.

The MW effects on the morphological structure of PCL/PVPh blends may indeed be well interpreted by the above growth rate postulate. Figure 7 shows the variation of crystal growth rate with M_{PCL}. The growth rate of the blend with M_{PCL} = 15 800 is obviously much

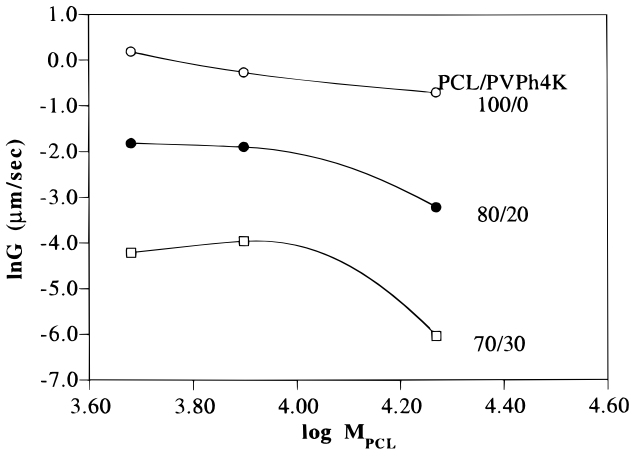

Figure 7. Effect of PCL molecular weight (M_{PCL}) on the crystal growth rate of PCL/PVPh4K blends. The growth rates of the blends with M_{PCL} = 15 800 are much lower than that of the blends with M_{PCL} = 2600 and 3800.

lower than that of the blends with M_{PCL} = 2600 and 3800. The slow crystal growth thus resulted in a larger extent of extralamellar segregation in PCL15K/PVPh blends. Because no considerable difference in growth rate is identified between the blends with M_{PCL} = 2600 and 3800, the extents of extralamellar segregation of these systems are about the same. Figure 8 demonstrates the influence of M_{PVPh} on the crystal growth rate. Despite the considerable difference between the two M_{PVPh} fractions investigated (4000 and 30 000), the growth rates of the blends with the two M_{PVPh} are approximately the same for a given composition. This may be ascribed to the interplay between the driving force and the mobility associated with crystallization. Decreasing M_{PVPh} could enhance the mobility associated with crystallization, but lower M_{PVPh} induced a larger entropy of mixing which depressed the driving force of crystallization by a larger extent. On the other hand, the higher M_{PVPh} induced a smaller depression of the driving force but imparted a greater difficulty for the PCL molecules to move. It is likely that the interplay between the two opposing factors resulted in the similar growth rate for the blends with the two M_{PVPh} fractions. Owing to the minor effect of M_{PVPh} on the growth rate, the extent of extralamellar segregation was essentially unaffected.

The present morphological investigation of PCL/PVPh blends has suggested that the crystal growth rate does play the most influential role in the morphological formation. This morphological principle may likely be applicable to other systems involving strong interactions. The morphological investigation of another strongly interacting system, PEO/PVPh blends, is currently underway. Our preliminary result shows that this system displays an even larger segregation distance, where PVPh is rejected into the interspherulitic region owing to the very slow crystal growth. The interspherulitic segregation gives rise to nonlinear growth of PEO spherulites.

Conclusions

The composition and molecular weight effects on the morphological patterns of PCL/PVPh blends have been investigated in this study. The presence of hydrogen bonding between the blending constituents led to the depression of equilibrium melting point and the forma-

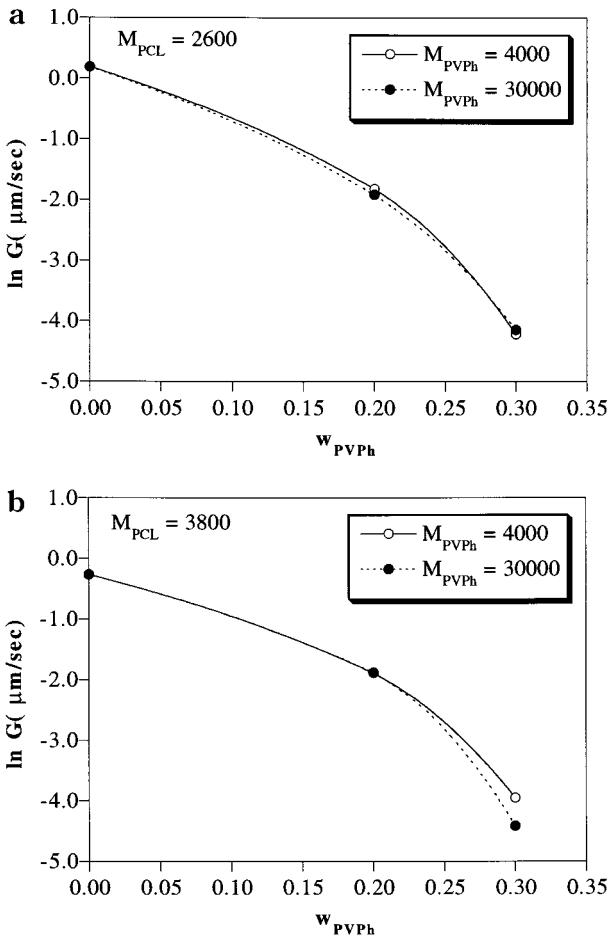

Figure 8. Composition variation of growth rate of (a) PCL2K/PVPh and (b) PCL3K/PVPh blends. For a given composition, the growth rate is relatively unaffected by the molecular weight of PVPh (M_{PVPh}) for the two M_{PVPh} fractions investigated.

tion of thicker PCL crystals in the blends. The extent of extralamellar segregation of PVPh was found to increase with PVPh composition but decreased with increasing PCL molecular weight. For the two MW fractions of PVPh investigated, the extent of extralamellar segregation was relatively unaffected by M_{PVPh}. Good correlations were found between the extent of extralamellar segregation and the crystal growth rate for the PCL/PVPh system, where slower growth rate led to higher extent of extralamellar segregation. The results supported a recent morphological principle suggesting that crystal growth rate plays the dominant role in the morphological formation of strongly interacting blends.

Acknowledgment. This work is supported by the National Science Council, R. O. C., under Grant NSC 88-2216-E-007-014.

References and Notes

(1) Stein, R. S.; Khambatta, F. B.; Warner, F. P.; Russell, T.; Escala, A.; Balizer, E. *J. Polym. Sci., Polym. Symp.* **1978**, *63*, 313.
(2) Russell, T. P.; Stein, R. S. *J. Polym. Sci., Polym. Phys. Ed.* **1982**, *20*, 1593.
(3) Russell, T. P.; Stein, R. S. *J. Polym. Sci., Polym. Phys. Ed.* **1983**, *21*, 999.
(4) Russell, T. P.; Ito, H.; Wignall, G. D. *Macromolecules* **1988**, *21*, 1703.
(5) Eersels, K. L. L.; Groeninckx, G.; Koch, M. H. J.; Reynaer, H. *Polymer* **1988**, *29*, 3893.
(6) Defieuw, G.; Groeninckx, G.; Reynaers, H. *Polym. Commun.* **1989**, *30*, 267.
(7) Defieuw, G.; Groeninckx, G.; Reynaers, H. *Polymer* **1989**, *30*, 595.
(8) Grevecoeur, G.; Groeninckx, G. *Macromolecules* **1991**, *24*, 1190.
(9) Hudson, S. D.; Davis, D. D.; Lovinger, A. J. *Macromolecules* **1992**, *25*, 1759.
(10) Huo, P. P.; Cebe, P.; Capel, M. *Mcromolecules* **1993**, *26*, 4275.
(11) Sauer, B. B.; Hsiao, B. S. *J. Polym. Sci., Polym. Phys. Ed.* **1993**, *31*, 901.
(12) Sadoco, P.; Canetti, M.; Seves, A.; Martuscelli, E. *Polymer* **1993**, *34*, 3368.
(13) Saito, H.; Stuhn, B. *Macromolecules* **1994**, *27*, 216.
(14) Cheung, Y. W.; Stein, R. S.; Lin, J. S.; Wignall, G. D. *Macromolecules* **1994**, *27*, 2520.
(15) Penning, J. P.; Manley, R. St. J. *Macromolecules* **1996**, *29*, 77.
(16) Talibuddin, S.; Wu, L.; Runt, J.; Lin, J. S. *Macromolecules* **1996**, *29*, 7527.
(17) Liu, L.-Z.; Chu, B.; Penning, J. P.; Manley, R. St. J. *Macromolecules* **1997**, *30*, 4398.
(18) Xing, P.; Dong, L.; An, Y.; Feng, Z.; Avella, M.; Martuscelli, E. *Macromolecules* **1997**, *30*, 2726.
(19) Talibuddin, S.; Runt, J.; Liu, L.-Z.; Chu, B. *Macromolecules* **1998**, *31*, 1627.
(20) Chen, H.-L.; Li, L.-J.; Lin, T.-L. *Macromolecules* **1998**, *31*, 2255.
(21) Keith, H. D.; Padden, F. J. *J. Appl. Phys.* **1964**, *35*, 1270.
(22) Debier, D.; Jonas, A. M.; Legras, R. *J. Polym. Sci., Polym. Phys. Ed.* **1998**, *36*, 2197.
(23) Moskala, E. J.; Varnell, D. F.; Coleman, M. M. *Polymer* **1985**, *26*, 228.
(24) Belfiore, L. A.; Qin, C.; Ueda, E.; Pires, A. T. N. *J. Polym. Sci., Polym. Phys. Ed.* **1993**, *31*, 409.
(25) Landry, M. R.; Massa, D. J.; Landry, C. J. T.; Teegarden, D. M.; Colby, R. H.; Long, T. E.; Henrichs, P. M. *J. Appl. Polym. Sci.* **1994**, *54*, 991.
(26) Chen, H.-L.; Li, L.-J.; Ou-Yang, W.-C.; Hwang, J. C.; Wong, W.-Y. *Macromolecules* **1997**, *30*, 1718.
(27) Strobl, G. R.; Schneider, M. *J. Polym. Sci., Polym. Phys. Ed.* **1980**, *18*, 1343.
(28) Debye, P.; Bueche, A. M. *J. Appl. Phys.* **1949**, *20*, 518.
(29) Debye, P.; Anderson Jr., H. R.; Brumberger, H. *J. Appl. Phys.* **1957**, *28*, 679.
(30) Ruland, W. J. *J. Appl. Crystallogr.* **1971**, *4*, 70.
(31) Santa Cruz, C. S.; Stribeck, N.; Zachmann, H. G.; Balta′ Calleja, F. J. *Macromolecules* **1991**, *24*, 5980.
(32) Stribeck, N.; Alamo, R. G.; Mandelkern, L.; Zachmann, H. G. *Macromolecules* **1991**, *24*, 5980.
(33) Albrecht, T.; Strobl, G. *Macromolecules* **1996**, *29*, 783.
(34) Cowley, J. M. *Diffraction Physics*, 2nd ed.; North-Holland: Amsterdam, 1981.
(35) Runt, J. P.; Zhang, X.; Miley, D. M.; Gallagher, K. P.; Zhang, A. *Macromolecules* **1992**, *25*, 3902.
(36) Oudhuis, A. A. C. M.; Thiewes, H. J.; van Hutten, P. F.; ten Brinke, G. *Polymer* **1994**, *35*, 3936.
(37) Lee, C. H.; Okada, T.; Saito, H.; Inoue, T. *Polymer* **1997**, *38*, 31.
(38) Hoffman, J. D.; Weeks, J. J. *J. Res. Natl. Bur. Stand. A: Phys. Chem.* **1962**, *66A*, 13.
(39) Hoffman, J. D.; Miller, R. L. *Polymer* **1997**, *38*, 3151.
(40) Lebedev, B.; Yevstropov, A. *Makromol. Chem.* **1984**, *185*, 1235.

MA9811019